J. Fluid Mech. (2010), *vol.* 662, *pp.* 197–208. © Cambridge University Press 2010
doi:10.1017/S0022112010003940

Self-consistent unstirred layers in osmotically driven flows

K. H. JENSEN[1]†, T. BOHR[2] AND H. BRUUS[1]

[1]Center for Fluid Dynamics, Department of Micro- and Nanotechnology, Technical University of Denmark, DTU Nanotech Building 345 East, DK-2800 Kongens Lyngby, Denmark

[2]Center for Fluid Dynamics, Department of Physics, Technical University of Denmark, DTU Physics Building 309, DK-2800 Kongens Lyngby, Denmark

(Received 29 January 2010; revised 21 July 2010; accepted 21 July 2010; first published online 27 September 2010)

It has long been recognized that the osmotic transport characteristics of membranes may be strongly influenced by the presence of unstirred concentration boundary layers adjacent to the membrane. Previous experimental as well as theoretical works have mainly focused on the case where the solutions on both sides of the membrane remain well mixed due to an external stirring mechanism. We investigate the effects of concentration boundary layers on the efficiency of osmotic pumping processes in the absence of external stirring, i.e. when all advection is provided by the osmosis itself. This case is relevant in the study of intracellular flows, e.g. in plants. For such systems, we show that no well-defined boundary-layer thickness exists and that the reduction in concentration can be estimated by a surprisingly simple mathematical relation across a wide range of geometries and Péclet numbers.

Key words: biological fluid dynamics, convection, membranes

1. Introduction

Osmotic transport characteristics of membranes are strongly influenced by the presence of unstirred concentration boundary layers adjacent to the membrane (Pedley 1983). As first demonstrated by Dainty (1963), these boundary layers lead to a decrease in the efficiency of the osmotic pumping process. To see this, consider an ideal semipermeable membrane (i.e. a membrane permeable to solvent molecules but impermeable to solute molecules) separating two solutions of the same solute at different bulk concentrations, say zero and unity, as shown in figure 1(*a*). If there were no transport of solvent across the membrane, these concentrations would persist all the way to the membrane. However, if there is a flux J of solvent due to osmosis across the membrane from the region of low concentration (say the left side) to the region of high concentration, the solutes will be pushed away from the membrane on the high-concentration side of the membrane. As a result, the concentration of solute in the vicinity of the membrane on the high-concentration side will be lower. The concentration difference between the two sides of the membrane is thus decreased, and this in turn reduces the magnitude of the osmotically driven flux J, which in the

† Email address for correspondence: kaare.hartvig.jensen@nanotech.dtu.dk

https://doi.org/10.1017/S0022112010003940 Published online by Cambridge University Press

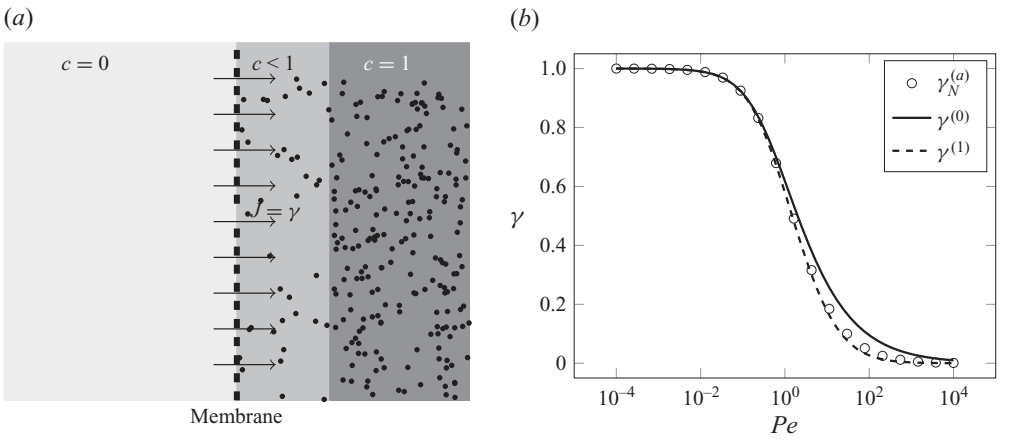


FIGURE 1. (*a*) Sketch of solute concentration distributions on either side of a semipermeable membrane separating two well-stirred solutions of the same solute at different bulk concentrations $c = 0$ (left side) and $c = 1$ (right side). Because of the transport of solvent across the membrane due to osmosis (sketched by the arrows) from left to right, there will be a tendency for the concentration γ of solute in contact with the membrane to be lower than unity just on the right side of the membrane. Since the flux of solvent J is proportional to the difference in concentration, we have that $J = \gamma$. (*b*) Numerically computed membrane concentration γ_N as a function of the Péclet number Pe for the parallel-plate geometry (circles) shown in figure 2(*a*). Also shown are the expressions given by (4.3) (solid) and (4.10) (dashed). See § 3 for details.

absence of hydrostatic pressure differences across the membrane is given by

$$J = \gamma, \tag{1.1}$$

according to the standard equations of non-equilibrium thermodynamics (Landau & Lifshitz 1980). Here, J is the volume flux per area per unit time, γ is the solute concentration immediately to the right (high concentration) side of the membrane, and both quantities are non-dimensional as described in § 2.1.

A large number of papers have presented both experiments (see e.g. Pohl 1998) and theory (see e.g. Pedley 1978, 1980, 1981, 1983; Aldis 1988) for the situation described above. Most of these workers have focused on the case where the solutions on both sides of the membrane remain well stirred such that a well-defined boundary layer exists. For a number of different geometries, the thickness of the boundary layer has been determined as a function of systems parameters, and the functional dependence on the osmotic pumping efficiency γ has been found.

A major limitation of the above theoretical and experimental work is, however, that it is concerned only with situations in which the solutions on both sides of the membrane remain well mixed due to an external stirring mechanism. In nearly all the cases, it is assumed that the flow generated by osmosis through (1.1) is negligible in determining the bulk flow, and only of significance close to the membrane.

The goal of the present work is to examine theoretically the situation in which the advecting bulk flow is itself driven by (1.1) and no external stirring is present. An important example, the one that inspired this work, is the flow in phloem cells of plants, where the osmotic pressure differences are believed to be responsible for the flow of the sugar solutions (the so-called Münch mechanism) (see e.g. Thompson & Holbrook 2003; Jensen *et al.* 2009). In this paper, we compute the concentration and flow profiles for various simple geometries. For these systems, we will show that no

https://doi.org/10.1017/S0022112010003940 Published online by Cambridge University Press

localized boundary layer exists, and second that the drop in concentration γ can be calculated by a simple mathematical relation valid across a wide range of geometries and Péclet numbers.

2. Governing equations and geometries

In the analysis of the problem described above, we shall consider steady osmotically driven flows confined between two infinite parallel plates at low Reynolds numbers. We thus consider systems such as those sketched in figure 2(*a–c*), and explained further in § 2.3, in which a solute of concentration c is diffusing and being advected by a velocity field $\boldsymbol{u}$, arising due to an osmotic flow across a membrane (indicated by dashed lines).

2.1. *Non-dimensional variables*

To simplify the mathematical expressions, we are using non-dimensional variables throughout this paper. The explicit scalings are: lengths are given by the plate-to-plate distance h; concentrations are in units of the characteristic concentration c_0; velocities are given by the characteristic osmotic velocity $u_0 = L_p RT c_0$, where L_p is the permeability of the membrane, R is the molar gas constant and T is the absolute temperature. Moreover, pressure is given in terms of shear-stress pressure $p_0 = \eta u_0 / h$.

The Reynolds number is given by $Re = \rho u_0 h/\eta \ll 1$, so we treat only Stokes flow in this paper. The Péclet number is given by $Pe = u_0 h/D$, where D is the diffusivity of the solute. In most cases, we assume that $Re \ll 1$, while Pe is finite which implies that the Schmidt number $Sc = \eta/\rho D$ is very large. This is consistent with the situation in plant cells, where the Schmidt number is of order 10^4.

2.2. *Steady-state equations of motion – Stokes flow*

The equations of motion governing the velocity field $\boldsymbol{u} = (u, v)$ and pressure field p are the Stokes equation and the continuity equation

$$\nabla p = \nabla^2 \boldsymbol{u}, \tag{2.1}$$

$$\nabla \cdot \boldsymbol{u} = 0. \tag{2.2}$$

The equation governing the concentration field is

$$\boldsymbol{u} \cdot \nabla c = \frac{1}{Pe} \nabla^2 c. \tag{2.3}$$

The velocity boundary condition at the membrane interface Ω is that the normal velocity component $\boldsymbol{n} \cdot \boldsymbol{u}$ is given by

$$\boldsymbol{n} \cdot \boldsymbol{u}(x, y) = c(x, y) \quad \text{for } (x, y) \in \Omega. \tag{2.4}$$

The concentration boundary condition is that the normal component of the solute flux across the membrane must be zero, i.e.

$$\frac{1}{Pe} \boldsymbol{n} \cdot \nabla c(x, y) + \boldsymbol{n} \cdot \boldsymbol{u}(x, y) c(x, y) = 0 \quad \text{for } (x, y) \in \Omega. \tag{2.5}$$

Solutions to (2.1)–(2.5) for arbitrary geometries are not readily available. Thus in § 3 we study full numerical solutions to our problem, and from the observed behaviour of these we establish and verify approximate analytical solutions in § 4.

https://doi.org/10.1017/S0022112010003940 Published online by Cambridge University Press

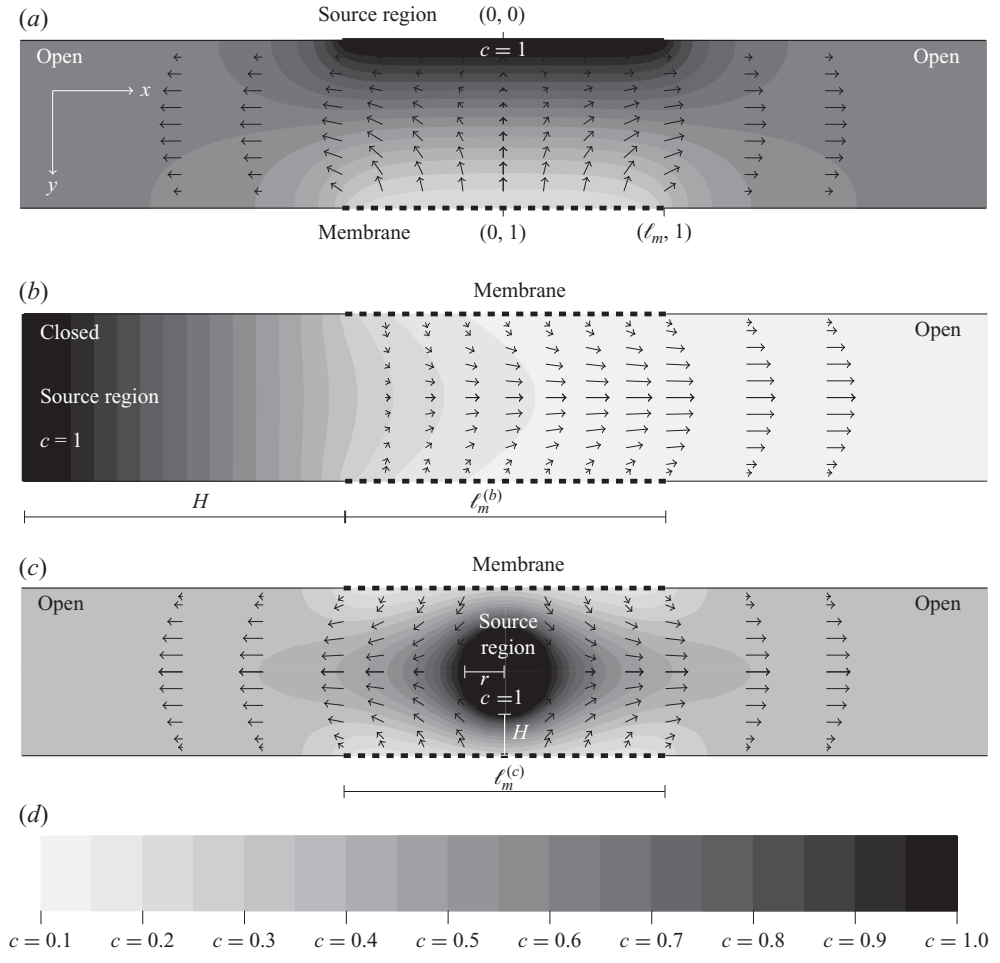


FIGURE 2. Sketch of the geometries considered. (*a*) Flow between parallel plates. On the upper plate, a region is kept at a constant concentration $c = 1$. On the lower plate, facing the constant concentration zone at distance $H = 1$, is a membrane of length $2\ell_m$ in this case plotted for $\ell_m = 1$. By osmosis, liquid flows across the membrane, thereby diluting the concentration near the membrane. (*b*) Flow between parallel plates with a membrane of length $\ell_m^{(b)} = 2$ at a right angle to the concentration source. The distance between the two zones is $H = 2$. (*c*) A cylinder of radius $r = 1/4$, embedded exactly half-way between the two plates. At the surface of the cylinder, the concentration is kept constant at $c = 1$. The length of the membrane zone is $\ell_m^{(c)} = 2$ and $H = 1/4$. In (*a*)–(*c*), numerically computed concentration contours (see (*d*)) are shown (plotted for $Pe' = 10$, see § 5). The velocity field is indicated by the arrows. (*d*) Contour scale bar for the concentration contour plots in (*a*)–(*c*).

2.3. *Geometries*

We consider the three geometries shown in figure 2. Outside the indicated membranes a solution of concentration $c = 0$ is present. First, in figure 2(*a*), left–right symmetric flow between two parallel plates separated a non-dimensional distance of 1 is analysed. At the upper plate, a source region of length $2\ell_m$ is kept at a constant concentration $c = 1$. On the lower plate, facing the constant concentration zone, is a membrane (indicated by the dashed line) also of length $2\ell_m$. Second, in figure 2(*b*), up–down

https://doi.org/10.1017/S0022112010003940 Published online by Cambridge University Press

symmetric flow between two parallel plates (separated by a distance 1) with a solid-wall source region ($c = 1$) at a right angle to the membrane is considered. The length of the membrane zone is $\ell_m^{(b)}$, and the distance from the source region to the membrane region is H. Finally, in figure 2(c), left–right and up–down symmetric flow around a solid cylinder of radius r embedded exactly half-way between two plates (separated by a distance 1) is considered. At the surface of the cylinder is a source region ($c = 1$). The length of the membrane zone is $\ell_m^{(c)}$. At the cylinder surface we impose a no-slip boundary condition.

In the following, we will investigate geometry (a) analytically and numerically, while geometries (b) and (c) will only be considered numerically.

3. Numerical results for the left–right symmetric parallel-plate problem

The steady-state behaviour of the systems shown in figure 2 was solved using the numerical methods described in Appendix A. The figure shows typical concentration and velocity profiles obtained in this way. Varying the Péclet number Pe, a number of such simulations were made and the following qualitative observations were made.

In geometry (a), for $Pe \ll 1$, the concentration in the membrane zone ($0 < x < \ell_m$) hardly varies at all along the x direction, and the variation along the y direction is linear. This is illustrated in figure 3 which shows cross-sections taken along the y direction at four different x values. For $x > \ell_m$ the concentration is flat, having been smoothed by diffusion. Near $x = \ell_m$ a transition takes place between the linear concentration gradient and the flat concentration plateau near the outlet. This is illustrated in figure 4, where cross-sections taken along the x direction are shown.

To quantify the efficiency of the osmotic pumping process, we calculate the mean concentration at the membrane γ as a function of the Péclet number Pe, plotted in figure 1(b). For small values of Pe, γ tends to the inlet concentration $c = 1$. This is reasonable since any depletion of the membrane concentration would be counteracted by the strong diffusion. For larger values of Pe, equilibrium between diffusive and advective forces leads to values of $\gamma < 1$ thus reducing the efficiency of the osmotic pump.

One further observation is, as shown in figure 3(e–f), that the velocity field $\boldsymbol{u} = (u, v)$ is well described by a squeeze flow (Bruus 2008):

$$u(x, y) = 6xy(1 - y)\gamma, \tag{3.1a}$$

$$v(x, y) = y^2(2y - 3)\gamma. \tag{3.1b}$$

Despite the richness found in the numerical solutions illustrated in figure 1(b) and figures 2–4, the system can be described theoretically using a few simple assumptions regarding the flow and velocity field at very low Péclet numbers. From there, the solutions can be extended using perturbation methods to be valid across a wider range of parameter values.

4. Theory for the left–right symmetric parallel-plate problem

Inspired by the qualitative results discussed above, we will begin by modelling the concentration profile of figure 2(a) using that for $Pe \ll 1$ the concentration profile is linear in the membrane zone. Near the outlet, the concentration profile is flattened by diffusion and the resulting concentration value is simply the mean of the values

https://doi.org/10.1017/S0022112010003940 Published online by Cambridge University Press

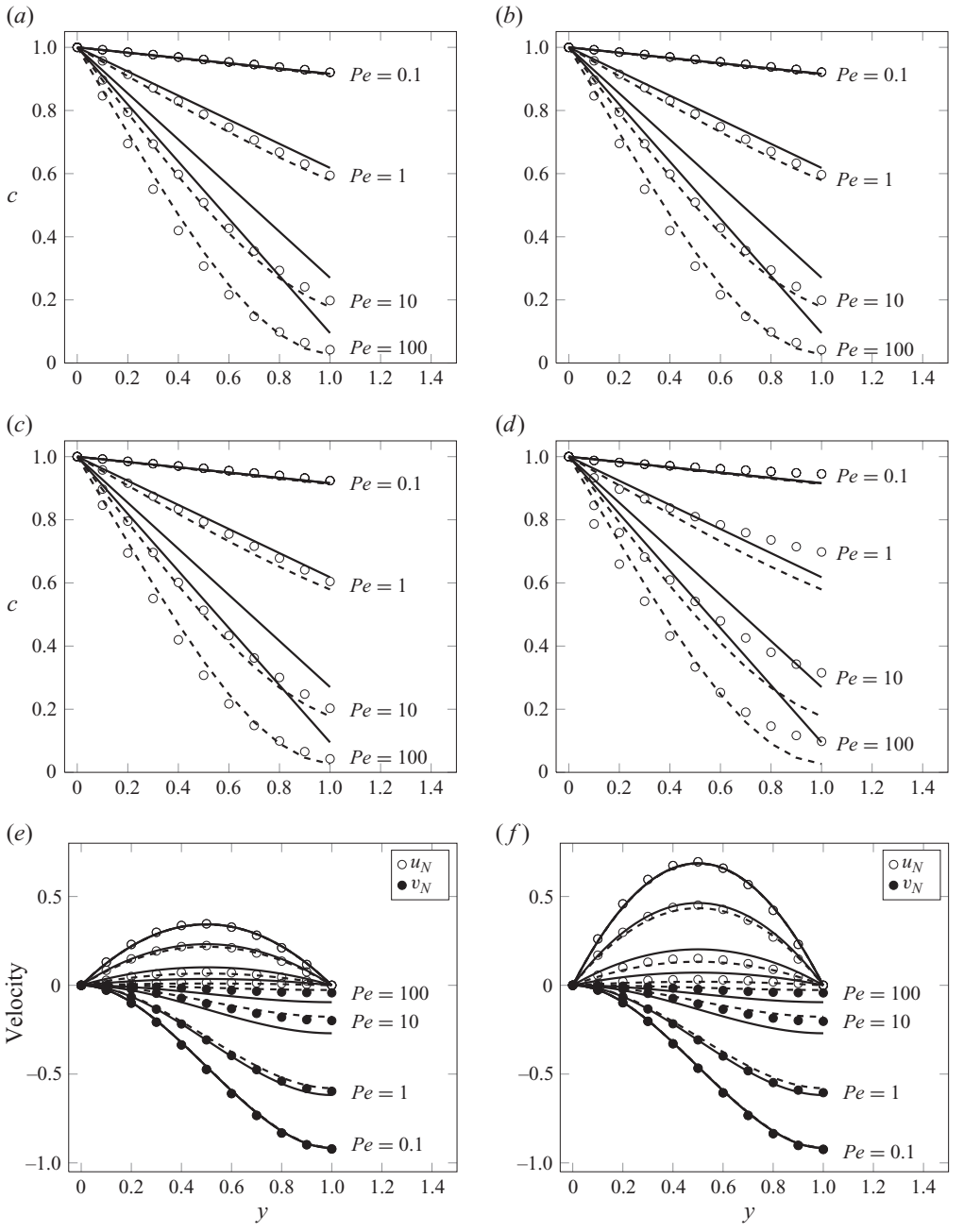


FIGURE 3. (*a–d*) Numerically computed concentration profiles c (circles) plotted against y for different values of x ($x=0$ (*a*), $x=0.25$ (*b*), $x=0.5$ (*c*), $x=1$ (*d*)) and the Péclet number Pe (as indicated next to the data points). All plots were obtained for the geometry in figure 2(*a*) with $\ell_m = 1$. Also shown are the expressions given by (4.1) (solid lines) and (4.9) (dashed lines). (*e*, *f*) Numerically computed velocity profiles u_N (open circles) and v_N (black circles) plotted against y for $x = 0.25$ (*e*) and $x = 0.5$ (*f*) and different values of the Péclet number Pe (as indicated next to the data points). Also shown are the velocity profiles given by (3.1*a*) and (3.1*b*) for u and v, respectively The solid lines are plotted with γ obtained from (4.3) while the dashed lines use $\gamma^{(1)}$ from (4.10).

https://doi.org/10.1017/S0022112010003940 Published online by Cambridge University Press

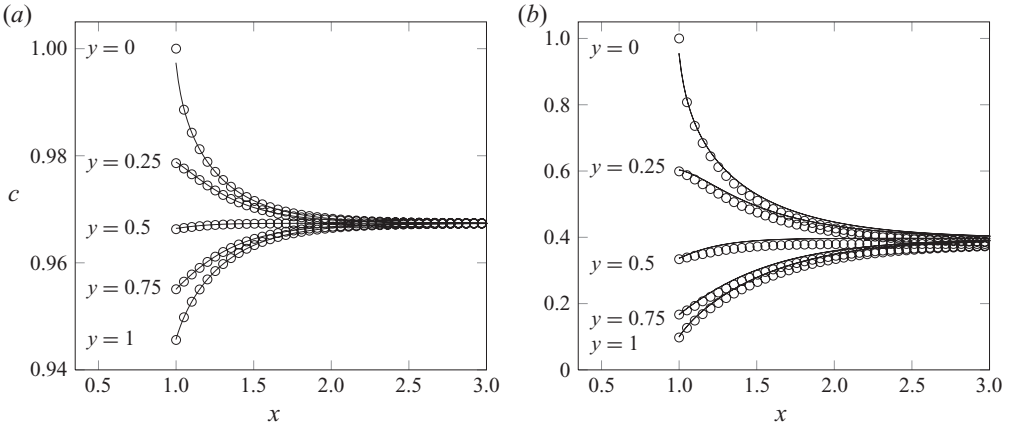


FIGURE 4. Numerically computed concentration profiles c (circles) plotted against x for different values of y (as indicated next to the plots) and the Péclet number Pe ($Pe = 0.1$ (a), $Pe = 100$ (b)). All plots were obtained with $\ell_m = 1$. Also shown is the expressions given by the solution to (4.11) (solid lines).

at the source region and at the membrane:

$$c(x, y) = \begin{cases} 1 - (1-\gamma)y & \text{for } x < \ell_m, \\ \frac{1}{2}(1+\gamma) & \text{for } x > \ell_m. \end{cases} \tag{4.1}$$

To estimate the concentration at the membrane γ, we use the boundary condition (2.5):

$$\frac{1}{Pe}\partial_y c = -\gamma^2. \tag{4.2}$$

With (4.1) this leads to

$$\gamma = \frac{\sqrt{1+4Pe}-1}{2Pe}, \tag{4.3}$$

an expression which does not, except for the length scale h in the Péclet number, depend on the specific geometry. Figure 1(b) shows the numerical results compared with (4.1) and (4.3).

4.1. *A detailed look at the concentration profile for $x < \ell_m$*

For $Pe \geqslant 1$, the assumption of a linear concentration profile given in (4.1) is no longer valid. To determine a more accurate concentration distribution in the membrane zone, we consider the equation governing the concentration field:

$$\partial_x^2 c + \partial_y^2 c = Pe(u\partial_x c + v\partial_y c). \tag{4.4}$$

Starting with the result from (4.1), we will expand the solution of (4.4) in powers of Pe as $c = c^{(0)} + Pe\,c^{(1)} + Pe^2 c^{(2)} + \ldots$, with

$$c^{(0)} = 1 - (1-\gamma)y. \tag{4.5}$$

To first order in Pe the governing equation becomes

$$\partial_x^2 c^{(1)} + \partial_y^2 c^{(1)} = u\partial_x c^{(0)} + v\partial_y c^{(0)}. \tag{4.6}$$

The boundary conditions are that $c = 1$ on the top boundary and that $c = \gamma$ on the membrane. We will assume that the terms $\partial_x^2 c^{(1)}$ and $u\partial_x c^{(0)}$ are small compared to

https://doi.org/10.1017/S0022112010003940 Published online by Cambridge University Press

$\partial_y^2 c^{(1)}$ and $v\partial_y c^{(0)}$. We further use that the velocity field $\boldsymbol{u} = (u, v)$ can be described by a squeeze flow. Inserting $c^{(0)}$, we get that

$$\begin{aligned}\partial_y^2 c^{(1)} &= v\partial_y c^{(0)} = \gamma y^2 (2y-3)\,[-(1-\gamma)] \\ &= -\alpha y^2(2y-3),\end{aligned} \tag{4.7a}$$

where $\alpha = \gamma(1-\gamma)$. Finally, $c^{(1)}$ becomes

$$c^{(1)} = -\frac{\alpha}{20}(2y^5 - 5y^4 + 3y). \tag{4.8}$$

Thus, to first order in Pe, the concentration distribution is

$$c(x, y) = 1 - (1-\gamma)y - \frac{\alpha Pe}{20}(2y^5 - 5y^4 + 3y). \tag{4.9}$$

The corresponding correction to γ calculated from the membrane boundary condition in (4.2) is

$$\gamma^{(1)} = \frac{\sqrt{\frac{49}{400}Pe^2 + \frac{33}{10}Pe + 1} - 1 - \frac{7}{20}Pe}{\frac{13}{10}Pe}, \tag{4.10}$$

which is shown as the dashed line in figure 1(*b*). To compare (4.9) and (4.10) with our numerical simulations, figure 3 shows numerically obtained concentration profiles plotted as a function of y along with (4.9) for $x = 0$, 0.25, 0.5 and $x = 1$.

4.2. *A detailed look at the concentration profile for $x > \ell_m$*

For $x > \ell_m$ we shall assume that the flow is parallel to the x-axis, such that the equation of motion is now

$$\partial_x^2 c + \partial_y^2 c = Pe\, u\partial_x c, \tag{4.11}$$

where u is now a parabolic velocity profile $u = 6\gamma y(1-y)\ell_m$ and $v = 0$. As c is even in y, we expand it in a cosine-series $c(x, y) = c_0 + \sum_{n=1}^{\infty} c_n(x)\cos(n\pi y)$ and the equation for the coefficients $c_n(x)$ has the form $\partial_x^2 c_n - n^2\pi^2 c_n - \sum_{m=1}^{\infty} A^{nm}\partial_x c_m = 0$, where the matrix elements A^{nm} are given in Appendix B. Truncating to the lowest two orders $(n, m = 1, 2)$, we search for the exponentially decaying solutions $c_i(x) = c_i^0 \exp(\lambda_i x)$ satisfying

$$\left(\lambda_1^2 - A^{11}\lambda_1 - \pi^2\right)\left(\lambda_2^2 - A^{22}\lambda_2 - 4\pi^2\right) = 0, \tag{4.12}$$

with negative values of λ_1 and λ_2. The most important eigenvalue is the one with the smallest absolute value since it will determine the asymptotic decay. It seems likely that this eigenvalue is associated with the lowest modes and thus it should be given as

$$\lambda^* = \tfrac{1}{2}\left(A^{11} - \sqrt{(A^{11})^2 + 4\pi^2}\right). \tag{4.13}$$

In the limit $Pe \ll 1$, we find that $\lambda^* \simeq -\pi$. Taking the first-order result (4.10), we find $Pe\gamma^{(1)} \to 20/7$ for $Pe \gg 1$, which implies that $A^{11} = (20/7)\ell_m(1 - 3/\pi^2)$. As long as ℓ_m is not too large (i.e. when $A^{11} \ll 2\pi$), we once again obtain $\lambda^* \simeq -\pi$. If on the other hand $A^{11} \gg 2\pi$, we find that $\lambda^* \to 7\pi^4\ell_m/(20(\pi^2 - 3)) \approx -4.96\ell_m$.

For $\ell_m = 1$ and $Pe = (0.1, 1, 10, 100)$, we find numerically among the first 10 eigenvalues $\lambda_N^* = (-3.11, -2.93, -2.47, -1.88)$ while (4.13), with (4.10) used for calculating γ, gives $\lambda^* = (-3.11, -2.95, -2.58, -2.38)$, only differing significantly at the fourth eigenvalue.

https://doi.org/10.1017/S0022112010003940 Published online by Cambridge University Press

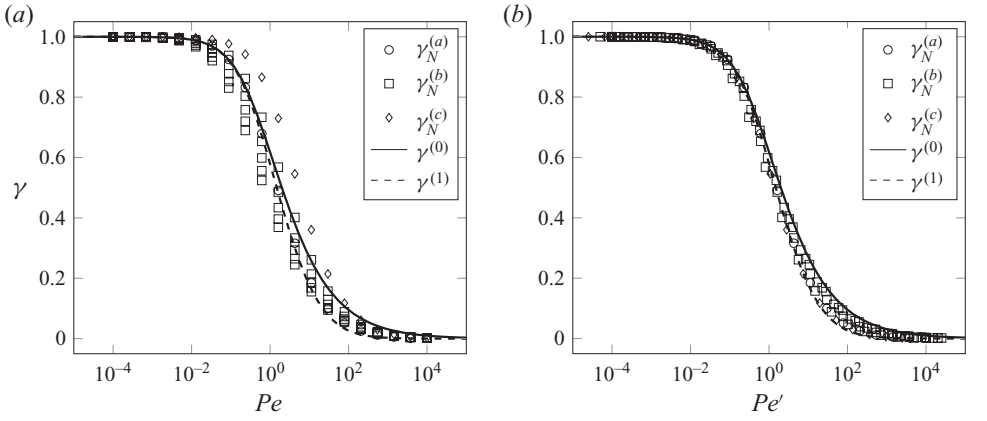


FIGURE 5. (*a*) Numerically computed mean membrane concentration γ_N as a function of the Péclet number $Pe = hu_0/D$ for the three geometries of figure 2. For geometry (*a*) plot of $\gamma_N^{(a)}$ for $H = 1$ (circles); for geometry (*b*) plot of $\gamma_N^{(b)}$ for H between 1/2 and 5/2 and $\ell_m^{(b)} = 1/2$ (squares); and for geometry (*c*) plot of $\gamma_N^{(c)}$ for $H = 1/4$, $\ell_m^{(c)} = 1/4$, and $r = 1/4$ (diamonds). The curves show the prediction given by (4.3) (solid curve) and (4.10) (dashed curve). (*b*) As in (*a*), except now γ_N is shown as a function of the modified Péclet number $Pe' = HPe = Hhu_0/D$.

5. Results from other geometries

To test the validity of (4.3) for geometries other than figure 2(*a*), for which it was originally derived, we show in figure 5 numerically obtained values of the mean membrane concentration γ_N plotted against Pe for the geometries found in figure 2(*b*) and (*c*). In figure 5(*a*), γ_N is plotted against the usual Péclet number, while in (*b*) it is plotted against the rescaled Péclet number

$$Pe' = \frac{Hhu_0}{D}, \tag{5.1}$$

where H is the minimum distance between the membrane and the constant concentration zone in units of the plate-to-plate distance h, as indicated in figures 2(*b*) and 2(*c*). As is clearly seen, the data collapse is significant when using Pe'. The result obtained in (4.10), while only valid for geometry (*a*), is shown for comparison.

The fact that the data collapse even for geometry (*b*) is surprising, since there the gradient from the source region to the membrane region is along the x direction and therefore (2.3)–(2.5), which even to lowest order in Pe constitute a highly nonlinear problem, do not directly reduce to (4.2). We interpret the data collapse as being due to the fact that the concentration gradient in the x direction induces a gradient of equal size in a direction normal to the membrane, in this case the y direction. This can be seen directly in figure 6, where the concentration x-derivative $\partial_x c$ is constant (-0.33 in this case) in the region separating the source and membrane zones, and equal to the y-derivative of the concentration $\partial_y c$ at the membrane interface.

This shows that the relative orientation of the source and membrane regions does not play a large role in determining the flow. This, however, is hardly surprising since one would not expect e.g. a change in orientation of the membrane to strongly influence the inflow at a given concentration, at least when the non-dimensional separation distance H is much larger than unity. The mathematical reason is presumably that the concentration field to lowest order in Pe satisfies the Laplace equation ((2.3) with $u = 0$) and thus that the integral of $(\nabla c)^2$ over the domain is

https://doi.org/10.1017/S0022112010003940 Published online by Cambridge University Press

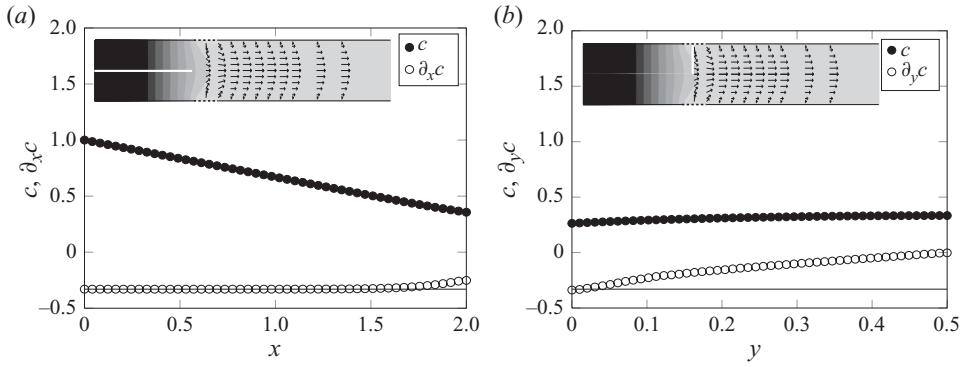


FIGURE 6. Flow and concentration field for geometry (*b*). (*a*) Cross-section plot of the concentration c (black circles) and the concentration x-derivative $\partial_x c$ (open circles) plotted along the solid white line shown in the inset for $H=2$, $\ell_m^{(b)}=1/2$ and $Pe'=10$. The solid black line indicates $\partial_x c=-0.33$. The concentration source is at $x=0$ and the membrane starts at $x=2$. (*b*) Cross-section plot of the concentration c (black circles) and the concentration y-derivative $\partial_y c$ (open circles) plotted along the solid white line shown in the inset for the same parameters as in (*a*). The solid black line indicates $\partial_y c=-0.33$, the value at the membrane ($y=0$).

minimal, favouring solutions where the size of the concentration gradient is nearly constant.

6. Conclusion

In this paper, we have studied new solutions to osmotically driven flow problems, where the distribution and fluxes of solutes and liquid have generated self-consistent flow and concentration patterns. We have presented a general analytical solution method, and have applied this method to a specific example, obtaining detailed knowledge of the flow- and concentration fields in the parallel-plate geometry (cf. figure 2*a*). This geometry has also been studied numerically, and we find good agreement between our analytical solution method and the numerics. Further, we have studied two topologically different geometries numerically varying the governing parameter, the Péclet number, by eight orders of magnitude. Using a scaled Péclet number, we obtain a data collapse over all eight orders of magnitude. This shows that while the detailed nature of the solutions depends on the geometry in question (cf. figure 2*a–c*), the osmotic pumping efficiency is largely independent of the geometry, as long as the correct length scale for the problem is chosen.

This work was supported by the Danish National Research Foundation, Grant No. 74.

Appendix A. Numerical methods

The problem posed by (2.1)–(2.5) was solved using the commercial finite element (FEM) software package COMSOL Multiphysics 3.4. See, for example, Jensen, Stone & Bruus (2006) for a detailed discussion of applying the FEM method to solve Stokes flow problems. To validate our numerical code, we used the analytical solution provided by Pedley (1981) for a shear flow above a membrane. Figure 7 shows a comparison between our numerical method and Pedley's analytical solution.

https://doi.org/10.1017/S0022112010003940 Published online by Cambridge University Press

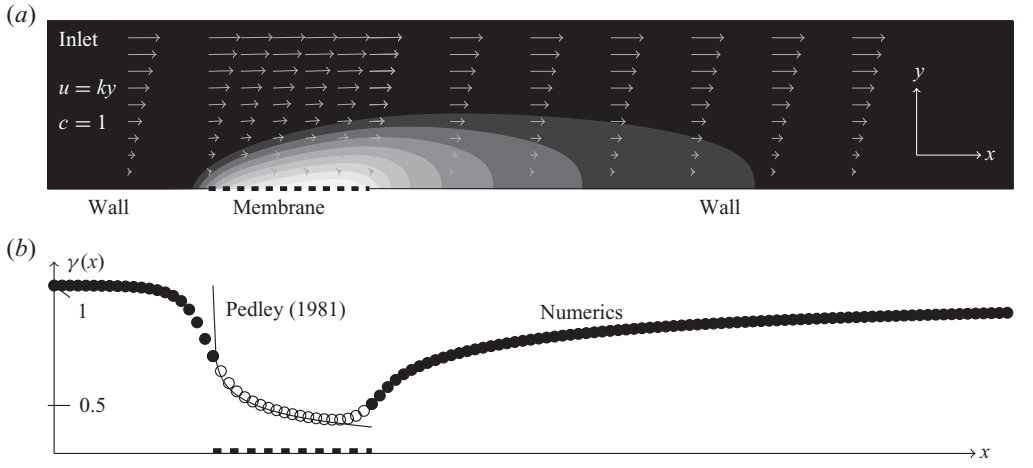


FIGURE 7. Comparison between our numerical method and Pedley's analytical solution for a shear flow above a membrane as shown in (*a*). To the left, a solution of concentration $c = 1$ is entering the computational domain with a velocity profile $(u, v) = (ky, 0)$. As the solution passes above the membrane, the flow and concentration profiles are perturbed, creating a characteristic boundary layer. Also shown in (*a*) are concentration contours (scale bar in figure 3*c*) and velocity arrow plot for $k = 25$ and $Pe = 10$. (*b*) Plot of the numerically computed concentration at the lower wall $\gamma(x)$ as a function of position x (open circles at the membrane, and solid circles on the wall). The solid line represents Pedley's analytical solution (Pedley 1981).

Appendix B. Solution of the diffusion–advection eigenvalue problem

The matrix elements A^{nm} in § 4.2 are

$$A^{nm} = 2\beta \int_0^1 \cos(n\pi y)\cos(m\pi y) y(1-y)\,\mathrm{d}y$$
$$= \begin{cases} -2\beta \dfrac{(1+(-1)^{m+n})(m^2+n^2)}{(m^2-n^2)^2\pi^2} & \text{for } n \neq m, \\ \dfrac{2\beta}{12}\left(1 - \dfrac{3}{n^2\pi^2}\right) & \text{for } n = m, \end{cases} \tag{B 1}$$

where $\beta = 6Pe\,\gamma\ell_m$. Note, that $A^{nm} = 0$ for odd values of $n + m$. The eigenvalue problem becomes the diagonalization of the matrix

$$\boldsymbol{M} = \begin{pmatrix} 0 & 1 & 0 & 0 & 0 & 0 & \cdots \\ 1^2\pi^2 & A^{11} & 0 & 0 & 0 & A^{13} & \cdots \\ 0 & 0 & 0 & 1 & 0 & 0 & \cdots \\ 0 & 0 & 2^2\pi^2 & A^{22} & 0 & 0 & \cdots \\ 0 & 0 & 0 & 0 & 0 & 1 & \cdots \\ 0 & A^{31} & 0 & 0 & 3^2\pi^2 & A^{33} & \cdots \\ \vdots & \vdots & \vdots & \vdots & \vdots & \vdots & \ddots \end{pmatrix}, \tag{B 2}$$

from which the coefficients c_n can be determined to obtain the solution to (4.11). Figure 4 shows the results for $N = 20$, $Pe = 0.1$ and $Pe = 100$ plotted together with the corresponding numerical solutions. Across the whole range of Pe values, we find good agreement with the numerical results.

https://doi.org/10.1017/S0022112010003940 Published online by Cambridge University Press

REFERENCES

Aldis, G. K. 1983 The unstirred layer during osmotic flow into a tubule. *Bull. Math. Bio.* **50**, 531–545.

Bruus, H. 2008 *Theoretical Microfluidics*. Oxford University Press.

Dainty, J. 1963 The polar permeability of plant cell membranes to water. *Protoplasma* **57**, 220–228.

Jensen, K. H., Hansen, R., Rio, E., Clanet, C. & Bohr, T. 2009 Osmotically driven pipe flows and their relation to sugar transport in plants. *J. Fluid Mech.* **636**, 371–396.

Jensen, M. J., Stone, H. A. & Bruus, H. 2006 A numerical study of two-phase Stokes flow in an axisymmetric flow-focusing device. *Phys. Fluids* **18** (3), 077103.

Landau, L. D. & Lifshitz, E. M. 1980 *Statistical Physics*. Pergamon.

Pedley, T. J. 1980 The interaction between stirring and osmosis. Part 1. *J. Fluid Mech.* **101**, 843–861.

Pedley, T. J. 1981 The interaction between stirring and osmosis. Part 2. *J. Fluid Mech.* **107**, 281–296.

Pedley, T. J. 1983 Calculation of unstirred layer thickness in membrane transport experiments: a survey. *Q. Rev. Biophys.* **16**, 115–150.

Pedley, T. J. & Fischbarg, J. 1978 The development of osmotic flow through and unstirred layer *J. Theor. Biol.* **79**, 427–447.

Pohl, P. 1998 The size of the unstirred layer as a function of the solute diffusion coefficient. *Biophys. J.* **75** (3), 1403–1409.

Thompson, M. V. & Holbrook, N. M. 2003 Application of a single-solute non-steady-state phloem model to the study of long-distance assimilate transport. *J. Theor. Biol.* **220**, 419–455.

https://doi.org/10.1017/S0022112010003940 Published online by Cambridge University Press